

Metal and Nonmetal Protective Screens for Hypervelocity Debris Shielding

**B.V. Rumyantsev^{1,*}, I.V. Guk², A.I. Kozachuk¹, A.I. Mikhailin², V.Y. Shevchenko³,
N.M. Silnikov², S.N. Perevislov³**

¹ A.F. Ioffe Institute of Physics and Technology of Russian Academy of Sciences, Politechnicheskaya ul., 26, 194021, St. Petersburg, Russia

² CJSC "NPO "Special Materials", B. Sampsonievskiy pr., 28a, 194044, St. Petersburg, Russia

³ NRC "Kurchatov Institute" - CRISM "Prometey", Shpalernaya ul., 49, 191015, St. Petersburg, Russia

Article history

Received December 19, 2022
Accepted January 11, 2023
Available online February 01, 2023

Abstract

The protective properties of metallic and nonmetallic screens were experimentally investigated when penetrated by an aluminum shaped charge jet at collision velocities of 7–10 km/s. Such a projectile is an analog of an elongated fragment of man-made debris. For materials of protective screens, we used glass, B₄C ceramics, and diamond-silicon carbide ceramic composite. The obtained results were compared with the data obtained for metal screens. In this paper, we show that the effectiveness of screen protection increases due to phase and structural transitions that occur during the interaction of elongated hypervelocity projectile with protective screens.

Keywords: hypervelocity impact; shaped charge jet; elongated aluminum projectile; protective screens; "IDEAL" composite ceramics

1. INTRODUCTION

The protection of spacecraft from space debris is becoming an increasingly urgent task every year [1–3] stimulating the ongoing research of the most efficient methods and materials for this task. The idea of screen protection against hypervelocity projectiles is based on the preliminary destruction of the projectile when interacting with a protective screen located at a distance in front of the rear barrier [4–6].

The most common material of man-made space debris is aluminum. The effectiveness of screen protection increases with an increase of the aluminum projectile velocity up to 7 km/s. With further increase in velocity from 7 km/s to 10 km/s, the ballistic limit remains constant and even decreases. It is related to the fact that at a velocity of 4 km/s melting of aluminum projectile is reached, and at a velocity of 7 km/s evaporation of the projectile happens [5,6], which leads to the increase in the intensity of destruction in the mentioned velocity

range. As a result of the impact of the projectile with a screen, molten and evaporated fragments of the projectile form. These fragments acquire a radial velocity component directed outward from the impact axis and disperse in inner screen space. They are partially absorbed by the screens and are excluded from the impact on protected structures [6]. Further increase in velocity above 7 km/s does not lead to new physical phenomena.

In this work, we investigate the efficiency of different materials for two-screen protection, with an emphasis on composite ceramics. In the experiments, an elongated aluminum projectile was formed with a specially calibrated shaped charge with an aluminum liner. The velocity of the obtained projectile was in the range characteristic of space debris in near-Earth orbit. Particular attention was paid to the effects of phase state changes of interacting materials at high impact velocities.

Most researches devoted to screen protection consider different variations of aluminum screens that are typically used in practice to protect spacecraft [5,6]. Recently, there

* Corresponding author: B.V. Rumyantsev, e-mail: brum@mail.ioffe.ru

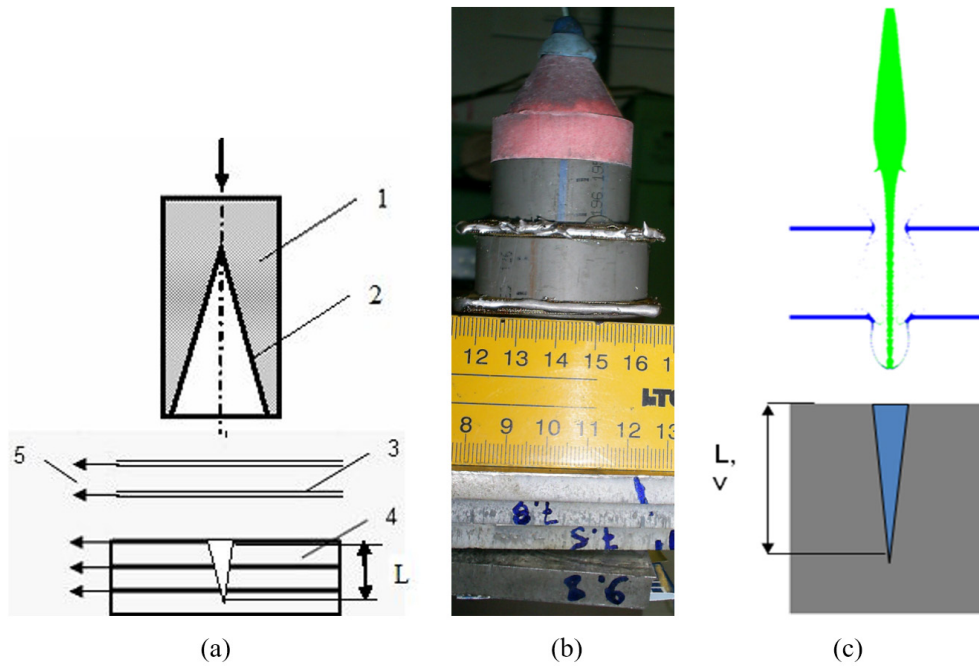


Fig. 1. (a) Experimental scheme: 1 – shaped charge, 2 – metal liner (the funnel), 3 – screens, 4 – barrier, 5 – contact sensors for time measurements; (b) photo of assembly; (c) numerical simulation of screens penetration and diagram of a cavern in a barrier. Damage parameters: L , v – cavern depth and volume.

is an interest in other technical solutions [7,8] and other types of materials, namely ceramic materials as part of composite screens [9,10].

Protective composite structures containing an outer ceramic layer are widely used to protect against bullets and shrapnel [11,12]. This utilizes such properties of ceramics as high hardness and high speed of sound. Concerning hypervelocity impacts, these properties of ceramics allow to increase the amplitude of shock waves that occur in the projectile when interacting with an obstacle. This leads to more intensive destruction of the projectile, which, in turn, leads to an increase in the angle of expansion and facilitates the processes of melting and evaporation of formed particles.

In this work, within the framework of a single methodological approach, the protective properties of screens made of metal, ceramics, and glass, with thick aluminum AMg6 barrier as a target, are compared when subjected to the impact of elongated aluminum projectiles with velocities of 10 km/s.

2. METHOD OF EXPERIMENT

The experimental scheme is shown in Fig. 1. To form the elongated projectile, shaped charges with an explosive mass (okfol) of 40 g were used. Shaped charges contained a metal liner in form of a funnel with a full angle at the top from 30 to 60 degrees, 0.08 cm thick, and with a 2 cm diameter at the base. The parameters of the pressed okfol (95/5 octogen/phlegmatizer): density is

1.75 g/cm³, detonation velocity is 8700 m/s, the heat of explosion 5.7 kJ/g. These shaped charges made it possible to obtain aluminum jets (elongated aluminum projectiles) with velocities up to 11 km/s.

Unlike widespread shaped charges with copper lining [13,14], charges 1 (Fig. 1) with aluminum alloy funnel 2 were used in the work. In other respects, the experimental technique was the same as in Refs. [15,16]. The elongated projectile obtained by detonating the shaped charge, penetrated protective screens 3 and embedded itself in the aluminum alloy (AMg6) barrier 4, forming a cavern in it. With contact sensors 5, the projectile velocity V_j was monitored during the penetration into the barrier.

Table 1 shows the parameters of aluminum shaped charge jets depending on the angle A of a 0.08 cm thick conical funnel made of AMg6. In further experiments, a short circuit with an aluminum funnel with an angle of 30° was used. In Table 1 parameters of shaped charge jets for different geometries and the results of their interaction with an AMg6 barrier at a focal length of 6 cm are presented. V_{j0} is the velocity of the head of the shaped charge

Table 1. Parameters of shaped charge jets interaction.

A , degrees	V_{j0} , km/s	L , cm	v , cm ³	D_j , cm ³
20	11.6	11.2	14	0.07
30	10.2	11.4	10.8	0.07
45	8.8	10	9.6	0.08
60	6.9	9.5	7.6	0.09

Table 2. Characteristics of brittle materials.

Material	Density, kg/cm ³	Elastic wave velocity, km/s		Hardness (<i>HV</i>), GPa	Bending strength, GPa
		C_l	C_t		
B ₄ C	2.52	14	8.8	30	0.44
Silicate glass	2.5	5.9	3.6	5.5	0.15
“IDEAL” ceramic	3.3	14.6	-	63–68	0.43–0.48

jet, the resulting penetration velocity is 3.7 km/s; L , v are the depth and volume of the cavern in the barrier without screen protection at a focal length of 6 cm; D_j is the average diameter of the projectile with a funnel thickness of 0.08 cm. In combination with the AMg6 barrier 4 (Fig. 1), the situation of the impact of man-made space debris with the screen protection of spacecraft was simulated in the experiments. The experiments were carried out in a vacuum chamber at a pressure of less than 1 kPa.

3. SELECTION OF MATERIALS USED FOR PROTECTIVE SCREENS

For protective screens, three significantly differing in mechanical properties brittle materials were used: boron carbide B₄C, silicate glass, and composite ceramic “IDEAL”. Their characteristics are presented in Table 2, where C_l is longitudinal speed of sound, C_t is transversal speed of sound, HV is Vickers hardness. Unlike boron carbide and silicate glass, the ceramic material, named “IDEAL” by its developers, is not very well known. This material is a composite with the ceramic silicon carbide (SiC) matrix filled with diamond particles. The data on the method of its preparation, structure, and properties are given below.

4. DIAMOND-SILICON CARBIDE COMPOSITE MATERIAL “IDEAL”

The following materials were used as initial components for composite ceramic “IDEAL”:

- a mixture of diamond powders with sizes of 20–28 microns (D_s) and 225–250 microns (D_b);
- black carbon (technical carbon);
- crushed silicon with average diameter $d_{0.5} = 1–2$ mm.

A composition with the component ratio of 30 vol.% D_s + 70 vol.% D_b was selected and composite diamond-silicon carbide ceramics were made with a reaction sintering process. The initial D_s and D_b powders in dry form were mixed in a drum mixer for 5 hours, with grinding bodies made of sintered SiC. The powder mixtures were plasticized with a 35% alcohol solution of phenol-formaldehyde resin and granulated by rubbing through a sieve with a mesh size of 0.3 mm.

Plasticized powders were dried in air at a temperature of 80 °C for 1 h. Samples with a size of 5×5×50 mm were pressed by semi-dry molding at a pressure of 100 MPa (compositions 1 and 2) and 50 MPa (composition 3). The sample blanks were dried in an air-drying cabinet at a temperature of 110 °C for 5 hours. Pyrolysis of phenol-formaldehyde resin was carried out in a vacuum furnace at a temperature of 800 °C for 5 hours.

During reaction sintering, the samples were placed in graphite containers and covered with silicon powder top. The impregnation process of the sample blanks was carried out in a vacuum furnace at a temperature of 1600 °C in a vacuum for 1 h.

According to Refs. [17–19], when liquid silicon is impregnated with porous blanks from diamond particles, a diamond-silicon carbide composite is formed according to the reaction-diffusion Turing mechanism [20]. At the first stage of impregnation, a thin layer of SiC is formed by contact of liquid Si with the carbon layer on the surface of diamond particles. Further reaction of silicon-carbon interaction is carried out by Si diffusion through the SiC layer. Consequently, the reaction process involves the diffusion of silicon atoms through the silicon carbide layer and the reaction between Si and carbon.

Accordingly, based on the reaction-diffusion Turing mechanism, nanoscale SiC grains form on the surface of diamond particles when gaseous Si diffuses into a porous workpiece. When liquid silicon is impregnated with a melt and pyrocarbon and diamond particles are dissolved, micron-sized SiC grains form, producing a Turing “fence” in both cases (Fig. 2).

The layering of silicon carbide onto diamond particles (the formation of Turing “fence”) leads to the enveloping of all diamond particles with dense layers of synthesized silicon carbide until the entire pore space in the diamond frame in the sample is filled and monolithic composite diamond-silicon carbide material is obtained (Fig. 3).

In areas rich in Si, the formation of SiC follows the dissolution-crystallization mechanism. The SiC grains crystallize on the diamond surface when carbon is cooled or saturated with liquid Si melt. Most often, for the impregnation process, Si is taken in excess concerning carbon. Carbon dissolves in the Si melt and diffuses into the

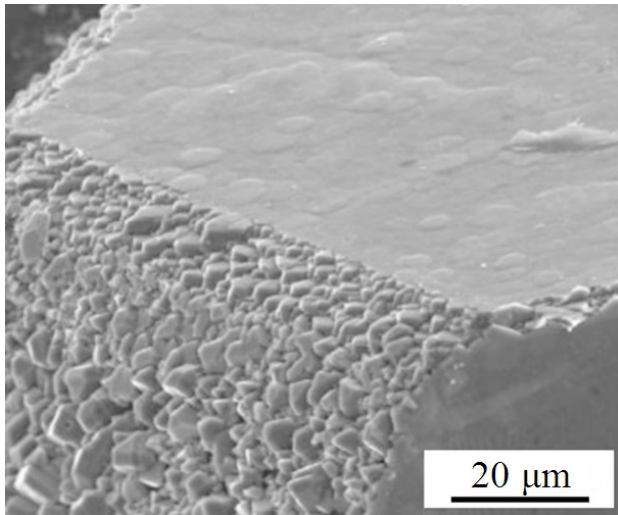


Fig. 2. Formation of micron-size SiC grains (Turing “fence”) on the surface of a diamond particle, during interaction of pyrocarbon with liquid Si.

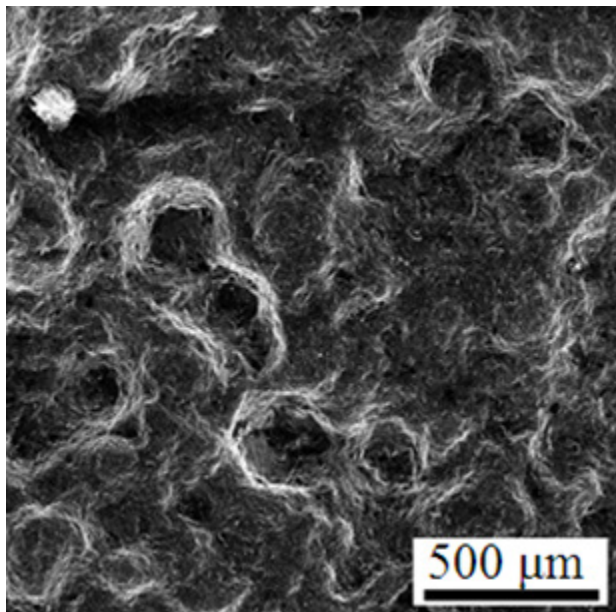


Fig. 3. Formation of SiC (Turing “fence”) layers on diamond particles in diamond–silicon carbide composite material.

cold zones of the material through the melt, where it becomes supersaturated in silicon. Micron-sized SiC grains precipitate and crystallize on the surface of diamond particles. The reaction rate is controlled by the concentration of carbon and its solubility in liquid Si [21].

The reaction-diffusion interaction of Si with carbon is accompanied by exothermic effects (a local increase in the system temperature to 2400 °C), with an enthalpy $H_0 = -117.77$ kJ/mol, which eliminates temperature gradients in the workpieces [22]. As a result, the Si diffusion rate increases several times, and the pores of the workpiece of diamond material are filled with SiC, which is formed as a result of the reaction-diffusion Turing mechanism.

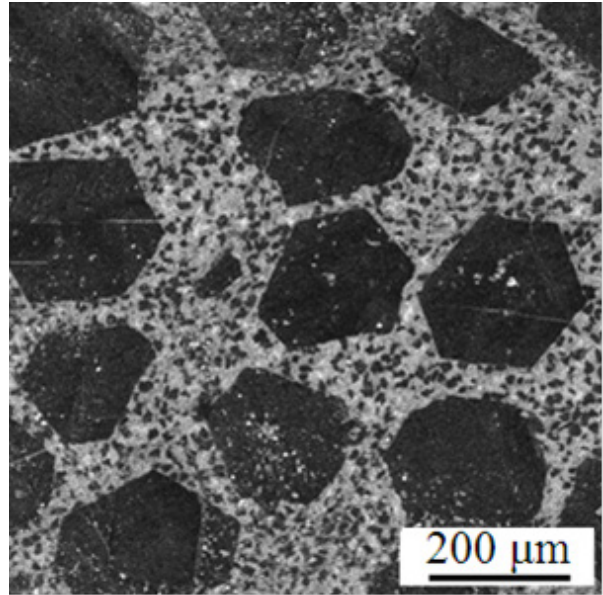


Fig. 4. Microstructure of diamond-silicon carbide composite.

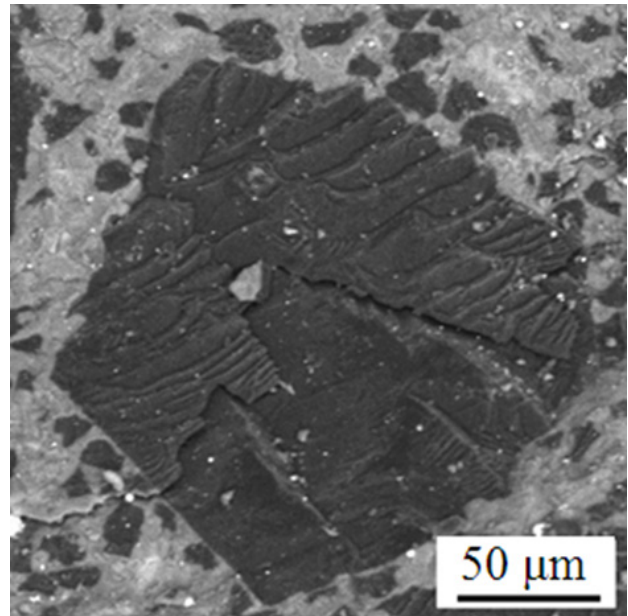


Fig. 5. Destruction of the diamond particle in diamond-silicon carbide composite.

Figure 4 shows the microstructure of the diamond-silicon carbide composite. Dark phases correspond to diamond particles, and the gray ones are β -SiC. Diamond crystals of the correct shape are uniformly distributed in the composite, which indicates that diamond crystals do not dissolve in Si during the impregnation process (reaction sintering). Figure 5 shows that diamond crystal in diamond-silicon carbide composite is destroyed by a transgranular mechanism. There are practically no pores in the material, which indicates a strong interfacial bond between diamond and SiC (Fig. 5).

Grains of β -SiC grow predominantly along the (111) crystallographic plane [23]. During impregnation, SiC

nucleation begins predominantly at the sites of defects on the diamond surface. Also, the nucleation of β -SiC grains depends on the structure of carbon-containing material (pyrocarbon, carbon black, graphite, etc.) introduced into the structure of the composite and obtained as a result of the pyrolysis of organic binders. Since diamond and silicon carbide are heterogeneous materials, when impregnating with liquid silicon, the Turing reaction-diffusion mechanism occurs, which makes it possible to synthesize silicon carbide without a clear transitional boundary between diamond and SiC particles.

The maximum compaction of workpieces can be achieved using initial diamond particles of the correct shape, for example, a truncated cube or a truncated octahedron. In this case, it is possible to obtain a reaction-sintered material consisting only of diamond particles and a silicon carbide phase. When certain conditions (concentration of components, impregnation temperature, medium pressure, etc.) are created for the reaction-diffusion interaction, SiC grains, predominantly octahedral in shape, are formed on the initial diamond particles (Fig. 4).

A very high level of mechanical characteristics can be achieved for materials characterized by high density and low porosity [24]. The determining factors influencing the density value of diamond-silicon carbide composite, provided that a practically pore-free material is obtained, are the same as for reaction-sintered silicon carbide [25]. They are the shape of the initial diamond particles, the accuracy of selected disperse composition of diamond powders (two-, three-fraction composition of powders), the optimal molding pressure of blanks. Having achieved such a result, the production of materials with maximum density and the highest level of mechanical characteristics is possible.

The resulting material, a diamond-silicon carbide composite called "IDEAL", surpasses classical materials — reaction-sintered silicon carbide [26,27] and reaction-sintered boron carbide [28,29] — in terms of mechanical characteristics. It can be expected that "IDEAL" will be effective as a protective material against hypervelocity impacts [30].

5. RESULTS OF THE EXPERIMENT

At the initial stage, basic characteristics of the destruction of the rear AMg6 barrier were determined in the absence of screens (Fig. 3). Figs. 6 and 7 show times and distances from the barrier surface during the projectile penetration, obtained with contact sensors. The data obtained earlier for metal screens are also presented there for comparison [31].

As noted earlier [31], copper screens show the greatest efficiency in the range of velocities from 7 to 10 km/s, which is associated with the evaporation of copper in the

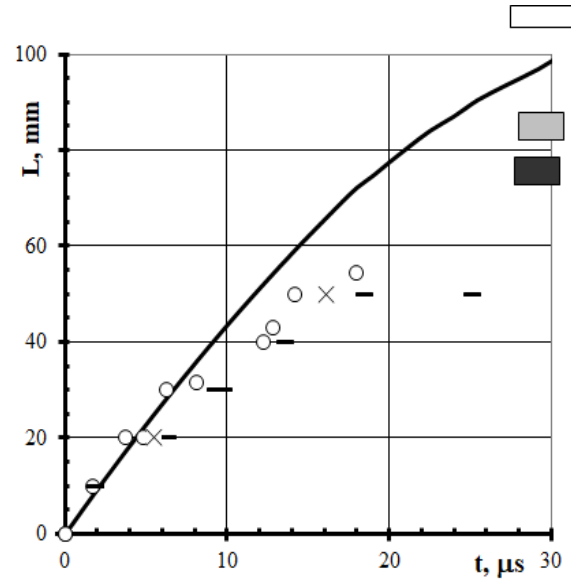


Fig. 6. Trajectories of elongated aluminum projectile penetration with an initial velocity of 10.2 km/s into AMg6 barrier. Symbols correspond to measured penetration times into barrier without screens (\circ), with AMg6 screens (\times) and copper screens ($-$). The rectangles are located at the final penetration level: light in absence of screens, dark in presence of copper screens, and AMg6 screens of equal weight (gray).

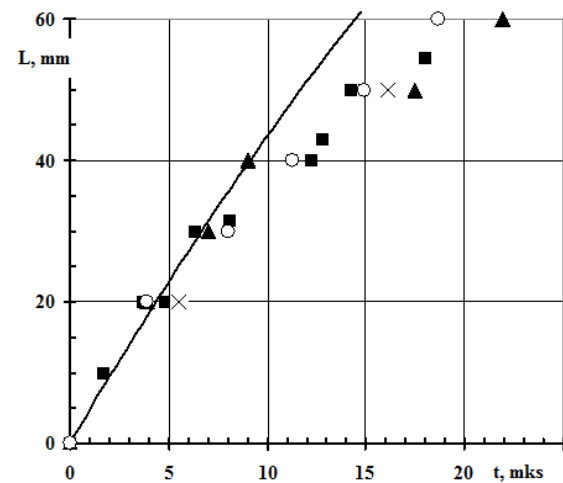


Fig. 7. Trajectories of elongated aluminum projectile penetration with an initial velocity of 10.2 km/s into AMg6 barrier without screens (\blacksquare), with two AMg6 screens (\times), two glass screens (\circ) and boron carbide screen (\blacktriangle). Screen thicknesses (surface density), and parameters of a cavern in the barrier are given in Table 1. The solid curve is the calculated trajectory of elongated projectile penetration in one-dimensional hydrodynamic approximation, with the strength of the barriers' material taken into the account [20].

projectile-screen interaction region [14]. The action of copper vapor destabilizes a significant part of the elongated projectile, which facilitates its dispersion on the way to the barrier.

The experimentally obtained characteristics of the penetration of elongated aluminum projectile into AMg6

Table 3. Parameters of protective screens and characteristics of projectiles' penetration into AMg6 barrier.

№	Screen material	Screen material density, g/cm ³	Number of screens	Total thickness, cm	m^* , g/cm ²	Depth of cavern L , cm	Cavern volume, cm ³	S_L	S_v
1	-	2.65	-	0	0	11.4±0.4	10.8±0.5	0	0
1**	-	2.65	-	0	0	9.5	7.6	0	0
2	AMg6	2.65	2	0.66	1.8	8.5	4.4	0.25	0.59
2**	AMg6	2.65	2	0.66	1.8	7.2	3.4	0.24	0.55
3	Copper M1	8.9	2	0.2	1.8	7.4	2.9	0.37	0.73
3**	Copper M1	8.9	2	0.2	1.8	5.2	2.7	0.45	0.64
4	Glass	2.5	2	0.72	1.75	8.6	6.2	0.24	0.48
5	B ₄ C	2.45	2	0.82	2.0	8.9	4.2	0.22	0.61
6	“IDEAL”	3.33	2	0.64	2.1	8.8	3.6	0.23	0.67
7	Glass	2.5	1	0.72	1.75	7.4	6.2	0.35	0.48
8	B ₄ C	2.45	1	0.75	1.8	8.9	4.2	0.11	0.61
9	“IDEAL”	3.33	1	1.0	3.3	5.5	3.6	0.52	0.69
10**	Stainless steel	7.8	2	0.22	1.7	5.2	3.0	0.45	0.61

barriers at impact velocities of 6.9 km/s (the number of the experiment is marked with ** in the Table 3) and 10.2 km/s (every other experiment) are summarized in Table 3. The effectiveness of screen protection was evaluated by a relative decrease in the barrier destruction parameters, such as depth S_L and volume S_v , in the presence of screens as follows:

$$S_L = 1 - L_i / L,$$

$$S_v = 1 - v_i / v,$$

where L_i and v_i are the depth and volume of the cavern in the barrier in the presence of screen protection, and L and v are the depth and volume of the cavern in the barrier in the absence of screens.

The results obtained for variants with one and two protective glass screens with the same total surface density gave the same value of the volumetric efficiency parameter S_v with a small gain in efficiency in terms of the linear parameter S_L . The effectiveness of screens made of glass turned out to be worse than all other materials.

When comparing two-screen protection scheme made of B₄C and “IDEAL” ceramic, “IDEAL” ceramic demonstrated the best results in terms of the volume parameter S_v . When comparing the linear parameter S_v , the efficiency of screens turned out to be the same, taking into account a slightly higher surface density m^* of “IDEAL” ceramic. The results for single and double B₄C screens with the same total area density showed the same efficiency. At the same time, the variant with one screen had a 10% lower surface density.

The S_L and S_v parameters used in this work can be interpreted as estimates of the comparative penetration

depth and the amount of absorbed energy when using various protective screens. For “IDEAL” ceramic, surface densities of one- and two-screen protection variants differed by a factor of one and a half. The difference in the volume parameter S_v for a massive screen does not exceed 3%. At the same time, according to the linear parameter S_L , for a more massive single screen, the result turned out to be 2.2 times better. If we accept that for screens made of “IDEAL” the effectiveness of single- and double-screen protection is close, as in the case of ceramics, it should be concluded that an increase in the thickness of a screen made of “IDEAL” ceramic significantly increases its protective properties.

The appearance of AMg6 barrier after interaction with the projectile, when one protective screen made of “IDEAL” ceramic was used, is shown in Fig. 8. It shows numerous traces of the interaction of screen fragments with the barrier over the entire area of the barrier. A similar picture is observed for B₄C screens. The results of computer simulation show that when an aluminum projectile penetrates boron carbide screens, the screens are destroyed with the formation of a compact flow of fragments (Fig. 9).

6. DISCUSSION OF THE RESULTS

The advantages of “IDEAL” ceramic in absorbing the projectile energy may be due to the presence of a structural phase transformation (diamond–graphite), which occurs with an increase in specific volume [33]. As in the case of copper evaporation, in the case of “IDEAL” ceramic during unloading, a phase insertion zone with a lower density occurs. This, in turn, has a perturbing effect on the projectile. Elongated projectile destabilizes and its fragments



Fig. 8. Entrance hole of the cavern (60 mm in diameter) in AMg6 barrier when hit by an aluminum projectile at 10 km/s with a single 3.2 mm “IDEAL” protective screen.

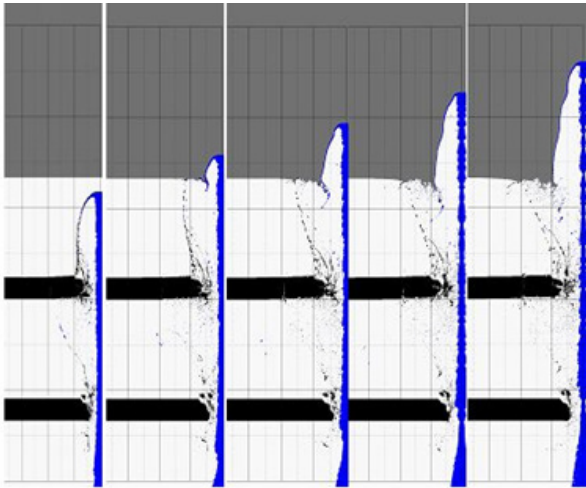


Fig. 9. Penetration of aluminum shaped charge jet with $V_{j0} = 10.2$ km/s through boron carbide screens into AMg6 barrier. Images are separated with an interval of 1 microsecond. Movement of the jet is from bottom to top, time is from left to right.

scattering in the interstitial space and in the cavern increases. Boron carbide comparable in strength has no modifications and/or inclusions with a significant change in density in the solid state [34] in the pressure range up to 50 GPa and, accordingly, the effectiveness of B_4C screen protection is lower.

Another reason for the effectiveness of “IDEAL” ceramic may be the higher Young’s modulus and, accordingly, the higher speed of sound. This should lead to an increase in spallation phenomena in the screens. In Ref. [32], when studying the dynamic strength of various grades of boron carbide ceramics under flat shock-wave loading, the registered velocities of free breakaway surface were 102–103 m/s. In the considered formulation of projectile penetration into a solid medium, the loading is not strictly one-dimensional and the breakaway occurs

from the walls of the cavity after unloading of penetrated area. It can be expected that in “IDEAL” ceramic, with higher than in boron carbide speed of sound, the role of spallation and breakaway destruction will increase. The higher speed of sound in “IDEAL” ceramic allows us to hope that its efficiency in comparison with boron carbide will remain even with an increase in the projectile velocity beyond 10 km/s.

One of the channels of energy dissipation of the projectile is the absorption of its kinetic energy due to the destruction of screens. In experiments with ceramic screens, their destruction was observed, in contrast to the destruction of a small area adjacent to the impact site of metal screens. The experimental scheme, where ceramic screens did not have a mechanically strong support layer, was used in the work. At the same time, it is well known that ceramic as a protective ballistic material works only in the presence of such a layer [11,12]. Such a scheme was used in Refs. [9,10]. The results obtained in those works show that at 10 km/s velocities ceramic itself is an effective protective material.

When using ceramic as an outer layer in composite screens, its acoustic impedance is of great importance. The excess of the screen impedance over the incoming projectile impedance makes it possible to increase the proportion of shock wave energy reflected from the screen and propagating through the projectile. Further, fragmentation of the projectile occurs under the influence of this shock wave. From this point of view, “IDEAL” ceramic is an exceptionally promising material, having an acoustic impedance four times higher than the acoustic impedance of aluminum.

In this work one shape of hypervelocity projectile — an elongated projectile — was experimentally considered. We acknowledge a limitation of such approach, as the work [35] has shown that different shapes of the projectile yield different results. Our future goal is to study, both numerically and experimentally, the interaction of variously shaped hypervelocity projectiles with screen protection made of “IDEAL”.

7. CONCLUSION

The levels of reduction of the elongated aluminum projectile destructive power at velocities of 10 km/s during the penetration of protective screens made of brittle materials such as glass, boron carbide (B_4C), and diamond-silicon carbide ceramic composite material “IDEAL” have been experimentally determined. The experiments were carried out on ceramic screens without a substrate. The best results in protecting the rear aluminum barrier under the impact of the projectile were shown by the “IDEAL” ceramic screens. This ceramic is a promising material for creating

composite organoceramic protective screens. A comparison of the newly obtained results with the data on the protective properties of metal screens confirms the conclusion that an important factor in increasing their efficiency is the use of phase transitions. These include melting, evaporation, and phase changes in the solid state. In particular, the rapid structural graphitization of the diamond phase into graphite in “IDEAL” ceramic screens, occurs under the influence of high pressures and temperatures during the interaction of the projectile and the screen.

REFERENCES

- [1] V. Adushkin, S. Veniaminov, S. Kozlov, M. Silnikov, *Orbital missions safety – A survey of kinetic hazards*, Acta Astronaut., 2016, vol. 126, pp. 510–516.
- [2] N.N. Smirnov (ed.), *Space Debris Hazard Evaluation and Mitigation*, Taylor and Francis Publ., London, 2002, 208 p.
- [3] N.N. Smirnov, A.B. Kiselev, A.I. Nazarenko, V.V. Tyurenkova, I.V. Usovik, *Physical and mathematical models for space objects breakup and fragmentation in hypervelocity collisions*, Acta Astronaut., 2020, vol. 176, pp. 598–608.
- [4] F.L. Whipple, *Meteorites and Space Travels*, Astronomical Journal, 1947, vol. 52, pp. 131.
- [5] K. Wen, X.-W. Chen, Y.-G. Lu, *Research and development on hypervelocity impact protection using Whipple shield: An overview*, Defense Technology, 2021, vol. 17, no. 6, pp. 1864–1886.
- [6] E.L. Christiansen, J. Arnold, A. David, J. Hyde, D. Lear, J.-C. Liou, F. Lyons, T. Prior, M. Ratliff, S. Ryan, F. Giovane, B. Corsaro, G. Studar, *Handbook for Designing MMOD Protection*, NASA, 2009.
- [7] M.N. Smirnova, K.A. Kondrat'ev, *Space debris fragments impact on multi-phase fluid filled containments*, Acta Astronaut., 2012, vol. 79, pp. 12–19.
- [8] M.V. Silnikov, I.V. Guk, A.F. Nechunaev, N.N. Smirnov, *Numerical simulation of hypervelocity impact problem for spacecraft shielding elements*, Acta Astronaut., 2018, vol. 150, pp. 56–62.
- [9] A. Cherniaev, I. Telichev, *Sacrificial bumpers with high-impedance ceramic coating for orbital debris shielding: A preliminary experimental and numerical study*, Int. J. Impact Eng., 2018, vol. 119, pp. 45–56.
- [10] S. Ren, R. Long, Q. Zhang, C. Chin, *The hypervelocity impact resistance behaviors of NbC/Al₂O₃ ceramic-metal composites*, Int. J. Impact Eng., 2020, vol. 148, art. no. 103759.
- [11] I.G. Crouch, *Introduction to armor materials*, in: I.G. Crouch (ed.), *The Science of Armor Materials*, Woodhead Publ., 2017, P. 33.
- [12] P.J. Hazell, *Armor. Materials, Theory, Design*. CRC Press, Boca Raton, 2016, P. 231.
- [13] L.P. Orlenko (ed.), *Explosion physics*, FIZMATLIT, Moscow, 2002, 656 p. ISBN 5-9221-0220-6 (in Russian).
- [14] C. Wang, J. Ding, H. Zhao, *Numerical Simulation on Jet Formation of Shaped Charge with Different Liner Materials*, Defence Science Journal, 2015, vol. 65, no. 4, pp. 279–286.
- [15] B.V. Rumyantsev, I.V. Guk, A.I. Kozachuk, A.I. Mikhailin, S.I. Pavlov, M.V. Silnikov, *Interaction between hypervelocity elongated projectile and screen protection of space vehicles*, Acta Astronaut., 2019, vol. 163, part. A, pp. 73–78.
- [16] B.V. Rumyantsev, A.I. Mikhailin, *Jet-charge as an effective tool in the development of spacecraft shields testing against micrometeoroids and man-made debris*, Acta Astronaut., 2015, vol. 109, pp. 166–171.
- [17] V.Ya. Shevchenko, M.V. Kovalchuk, A.S. Oryshchenko, S.N. Perevislov, *New chemical technologies based on Turing reaction–diffusion processes*, Doklady Chem., 2021, vol. 496, no. 2, pp. 28–31.
- [18] V.Ya. Shevchenko, S.N. Perevislov, V.L. Ugolkov, *Physicochemical interaction processes in the carbon (diamond)–silicon system*, Glass Phys. Chem., 2021, vol. 47, no. 3, pp. 197–208.
- [19] V.Ya. Shevchenko., S.N. Perevislov, *Reaction–diffusion mechanism of synthesis in the diamond–silicon carbide system*, Russ. J. Inorg. Chem., 2021, vol. 66, no. 8, pp. 1107–1114.
- [20] A. Turing, *The chemical basis of morphogenesis*, Phil. Trans. R. Soc. Lond. B, 1952, vol. 237, no. 641, pp. 37–72.
- [21] C. Zollfrank, H. Sieber, *Microstructure evolution and reaction mechanism of biomorphous SiSiC ceramics*, J. Am. Ceram. Soc., 2005, vol. 88, no. 1, pp. 51–58.
- [22] V.Ya. Shevchenko, M.V. Koval'chuk, A.S. Oryshchenko, *Synthesis of a new class of materials with a regular (periodic) interconnected microstructure*, Israel J. Chem., 2020, vol. 60, no. 5–6, pp. 519–526.
- [23] J.S. Park, R. Sinclair, D. Rowcliffe, M. Stern, H. Davidson, *Orientation relationship in diamond and silicon carbide composites*, Diamond Relat. Mater., 2007, vol. 16, no. 3, pp. 562–565.
- [24] V.Ya. Shevchenko, *Introduction to technical ceramics*, Nauka, Moscow, 1993, 114 p. ISBN 5-02-001644-6 (in Russian).
- [25] W.F. Knippenberg, *Growth phenomena in silicon carbide*, Philips Res. Report, 1963, vol. 18, pp. 161–274.
- [26] D.D. Nesmelov, O.A. Kozhevnikov, S.S. Ordan'yan, S.N. Perevislov, *Precipitation of the eutectic Al₂O₃–ZrO₂(Y₂O₃) on the surface of SiC particles*, Glass Ceram., 2017, vol. 74, no. 1, pp. 43–47.
- [27] S.N. Perevislov, T.L. Apukhtina, A.S. Lysenkov, M.G. Frolova, M.V. Tomkovich, *Effect of SiC fiber content in silicon carbide material on its mechanical properties*, Glass Phys. Chem., 2022, vol. 48, no. 1, pp. 54–60.
- [28] S.N. Perevislov, A.S. Lysenkov, S.V. Vikhman, *Effect of Si additions on the microstructure and mechanical properties of hot-pressed B₄C*, Inorg. Mater., 2017, vol. 53, no. 4, pp. 376–380.
- [29] S.N. Perevislov, P.V. Shcherbak, M.V. Tomkovich, *Phase composition and microstructure of reaction-bonded boron-carbide materials*, Refract. Ind. Ceram., 2018, vol. 59, no. 2, pp. 179–183.
- [30] V.Ya. Shevchenko, A.S. Oryshchenko, S.N. Perevislov, M.V. Sil'nikov, *About the criteria for the choice of materials to protect against the mechanical dynamic loading*, Glass Phys. Chem., 2021, vol. 47, no. 4, pp. 281–288.
- [31] B.V. Rumyantsev, I.V. Guk, A.I. Kozachuk, A.I. Mikhailin, S.I. Pavlov, M.V. Sil'nikov, *Possibilities of screen protection of space objects from an elongated impactor with a speed of 7–11 km/s*, Tech. Phys. Lett., 2021, vol. 47, no. 5, pp. 409–412.
- [32] A.S. Savinykh, G.V. Garkushin, S.V. Razorenov, V.I. Rumyantsev, *Dynamic strength of reaction-sintered boron*

- carbide ceramics, *Tech. Phys.*, 2015, vol. 60, no. 6, pp. 863–868.
- [33] V.B. Romanov, M.A. Rumyantsev, *The equation of state of carbon in problems of shock compression at a pressure of ~ 1 Mbar for graphite-like and diamond-like phases*, Brief communications on physics FIAN, 1997, no. 3–4, pp. 9–24 (in Russian).
- [34] P.A. Pokatashkin, *Molecular dynamics study of the mechanical properties of boron-saturated compounds with an alfa-bora type structure*, Thesis, FGUP VNIIA, 2018, 107 p (in Russian).
- [35] M.V. Silnikov, I.V. Guk, A.I. Mikhaylin, A.F. Nechunaev, B.V. Rumyantsev. *Numerical simulation of hypervelocity impacts of variously shaped projectiles with thin bumpers*, *Mater. Phys. Mech.*, 2019, vol. 42, no. 1, pp. 20–29.

УДК 623.438.3

Металлические и неметаллические экраны для защиты от высокоскоростного мусора

Б.В. Румянцев¹, И.В. Гук², А.И. Козачук¹, А.И. Михайлин², В.Я. Шевченко³,
Н.М. Сильников², С.Н. Перевислов³

¹ ФГБУ Физико-технический институт им. А.Ф. Иоффе Российской академии наук, Политехническая ул., 26, 194021, Санкт-Петербург, Россия

² АО «НПО Специальных материалов», Большой Сампсониевский пр., 28а, 194044, Санкт-Петербург, Россия

³ НИЦ «Курчатовский институт» - ЦНИИ КМ «Прометей», Шпалерная ул., 49, 191015, Санкт-Петербург, Россия

Аннотация. Защитные характеристики металлических и неметаллических экранов были экспериментально изучены при поражении алюминиевой кумулятивной струей со скоростями столкновения 7–10 км/с. Такой ударник является аналогом удлиненного фрагмента космического мусора. Для материалов защитных экранов были использованы стекло, карбид бора и керамический композиционный материал алмаз-карбид кремния. Произведено сравнение полученных результатов с данными для металлических экранов. В статье показано, что эффективность экранной защиты увеличивается из-за фазовых и структурных переходов, которые происходят при взаимодействии удлиненного высокоскоростного ударника с защитными экранами.

Ключевые слова: высокоскоростное столкновение; кумулятивная струя; удлиненный алюминиевый ударник; защитные экраны; композитная керамика «Идеал»